

# Volcanics from the South China Sea ridge system

Volcanism  
Petrology  
China Sea ridge  
Manila trench

Volcanisme  
Pétrologie  
Dorsale Mer de Chine  
Fossé de Manille

Roger HÉKINIAN <sup>a</sup>, Philippe BONTÉ <sup>b</sup>, Guy PAUTOT <sup>a</sup>, Dario JACQUES <sup>c</sup>,  
Laurent D. LABEYRIE <sup>b</sup>, Naja MIKKELSEN <sup>d</sup>, Jean-Louis REYSS <sup>b</sup>

<sup>a</sup> Institut Français de Recherche pour l'Exploitation de la Mer (IFREMER), Centre de Brest, B.P. 70, 29263 Plouzané, France.

<sup>b</sup> Centre des Faibles Radioactivités, Laboratoire mixte CNRS/CEA, Domaine du CNRS, 91190 Gif-sur-Yvette, France.

<sup>c</sup> Université de Bretagne Occidentale, Département de Géologie, 6 avenue Le Gorgeu, 29283 Brest Cedex, France.

<sup>d</sup> Geological Survey of Denmark, Thoravej 8, 2400 Copenhagen, Denmark.

Received 4/1/88, in revised form 26/5/88, accepted 30/11/88.

## ABSTRACT

Several seamounts (3) from the China Sea ridge system (Scarborough Seamount chain), as well as from the Eastern Wall of the Manila Trench where the ridge is being subducted, have been mapped (Seabeam) and sampled. Alkali basalts, trachybasalts, trachytes, and hyaloclastites were collected from sites located near 15°-116°E at 3000-3800 m depth. The range in compositional variations expressed in terms of Mg# (28-60), mineralogy and light lithophile element distribution (Ba = 130-480 ppm; Sr = 300-700 ppm; Rb = 35-110 ppm) indicates that crystal fractionation processes of the similar parental magma enriched (La/Sm)<sub>N</sub> ratio (2-2.5) have resulted in the various rock types. In addition, the heterogeneous nature of the crustal material beneath the seamounts is emphasized by the presence of foreign inclusions comprising websterite, werlites, gabbroic fragments, Na-plagioclase (an<sub>46</sub>) and Mg-rich (Fo<sub>85-88</sub>) and Mg-poor (Fo<sub>77-79</sub>) olivine which are brought to the surface solely with the various types of volcanic activity. The compositional variability and textural features of these foreign inclusions suggest that they are cumulates that formed as fractionation (Na-plagioclase) products during the upwelling of separate magmatic events. Age-dating performed on the calcareous nannofossils found in the hyaloclastites and sediments associated with the extrusives indicates that volcanic activities of the Scarborough ridge system in the area of sampling terminated during the late Miocene (11 m.y.) period.

*Oceanologica Acta*, 1989, 12, 2, 101-115.

## RÉSUMÉ

### Volcans de la dorsale de Mer de Chine

Trois volcans sous-marins de la dorsale de la Mer de Chine (chaîne de Seamounts-Scarborough) et un autre volcan situé sur le flanc (est) en subduction du fossé de Manille ont été cartographiés et échantillonnés pendant deux campagnes océanographiques du N.O. Jean Charcot (1984 et 1985) près de 15° Sud et 116° Est. Les roches prélevées sur ces volcans sous-marins par 3000-3800 mètres de profondeur sont constituées de basaltes alcalins, de basaltes trachytiques, de trachytes et de hyaloclastites. Les variations de compositions exprimées en terme de Mg# (28-60), de la minéralogie, et des teneurs en éléments lithophiles légers (Ba = 130-480 ppm; Sr = 300-700 ppm; Rb = 35-110 ppm) suggèrent une origine pour les différentes laves par un processus de cristallisation fractionné à partir d'une même source parentale enrichie dans le rapport (La/Sm)<sub>N</sub> (2-2.5).

La présence d'inclusion de roches (xénolithes de websterites, werlites et gabbros) et de minéraux (xénocristaux de plagioclase sodique et d'olivine) indique la nature hétérogène de la croûte sous-jacente à ces volcans sous-marins.

Les inclusions des roches représentent des cumulats formés par un magma différent de celui qui est à l'origine des laves alcalines. D'après les datations faites à partir des nanfossiles associés avec les coulées, il semblerait que l'activité volcanique au niveau des Seamounts de la chaîne Scarborough ait cessé pendant le Miocène tardif c'est-à-dire il y a environ 11 millions d'années.

*Oceanologica Acta*, 1989, 12, 2, 101-115.

## INTRODUCTION

The South China Sea is the largest of the marginal basins of the western Pacific. It is bordered by the passive continental margins of South China, Vietnam and Borneo and by the active margin of the Philippines bordering the Manila trench. In the central part of the basin, a 700 km-wide oceanic basin is characterized by east-west trending magnetic anomalies. Anomalies 11 to 5e (Taylor, Hayes, 1983) corresponding to an age of formation for the China basin comprised between 32 and 17 m.y. were identified. Near the latitude 15°N an east-west trending elongated ridge represents the extinct axis of an accreting plate boundary which is now subducting into the Manila trench (Hayes, Lewis, 1985). This ridge is capped by a chain of seamounts and reefs known as the Scarborough seamount chain (Hayes, Lewis, 1985). A recent morphological study based on Seabeam mapping and single channel seismic

reflection profiling (Pautot *et al.*, 1986) reveals a structural fabric in a NW-SE spreading direction. The structure of the ridge is disrupted at its intersection with the Manila trench near 15°50'N (Lewis, Hayes, 1985).

Very little is known about the composition of the crust in the South China Sea. In 1979 (Vema cruise 36) three dredges containing alkali basalts were collected on three seamounts of the Scarborough chain and the results of the major element analyses were reported by Taylor and Hayes (1983).

In this paper we present the results of four new dredges collected during two cruises of RV Jean Charcot in 1984 (Estase cruise) and in 1985 (Nanhai cruise). Three dredges are from the western part of the Scarborough chain (116°E latitude) near the junction with the S.W. basin and one dredge (EST DR1) was collected on the eastern part of the ridge where it is subducting into the Manila trench (China Sea side of the trench; Fig. 1). The detailed petrological descriptions of extrusive flows

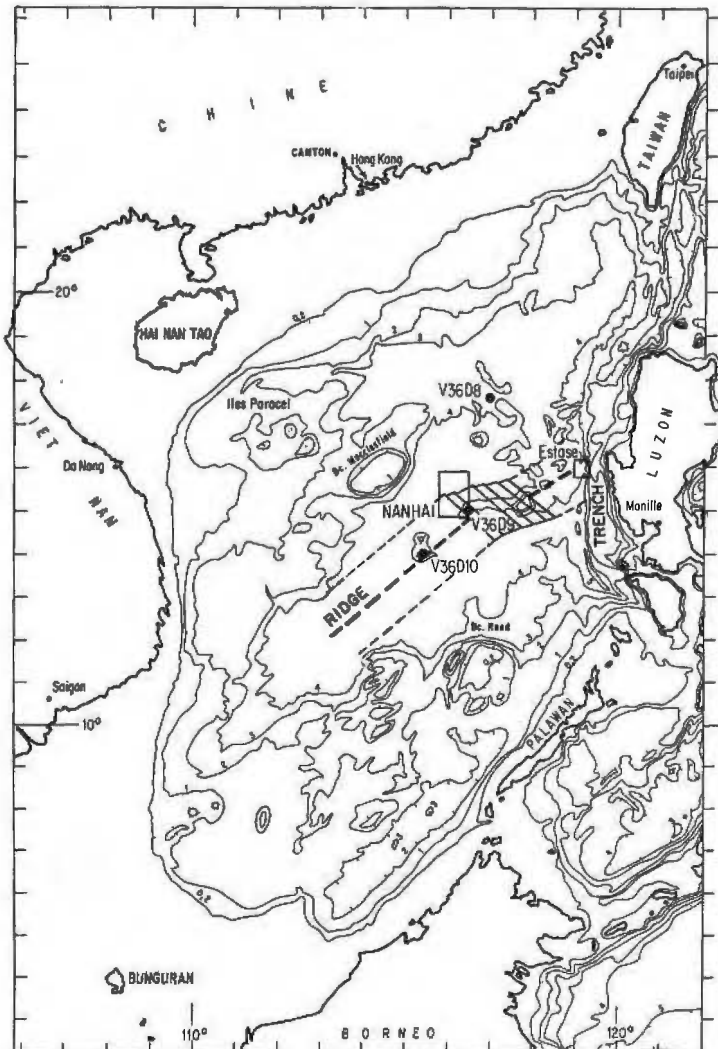


Figure 1

General bathymetric map of the China Sea showing the two zones sampled during the Estase (1984) and the Nanhai (1985) cruises of the R/V Jean Charcot. The black dots represent the sampling locations carried out during the Vema 36 cruise.

and intrusive xenoliths in relation to their geological settings obtained from Seabeam and seismic profiling are used to obtain a better insight into the magmatic processes involved in the formation and evolution of the China ridge system.

## GEOLOGICAL SETTING

Dredge hauls from the Nanhai cruise (NAN DR1, 2, 3) were collected from a region situated at the junction of two ridge systems, an E-W trending segment surrounded by the Scarborough seamounts and a more linear NE-SW trending segment which extends between the Vietnamese margin and Borneo (Pautot *et al.*, 1986; Fig. 1). From the Seabeam bathymetric map and seismic reflection data it is observed that the region consists of elongated seamounts surrounded by a sedimented bottom cover reaching 1 sec. d.t. thickness (Fig. 3, 4). Four main zones are recognized within the studied areas, the first three being in the Nanhai area:

1) the southwestern zone with a NE-SW elongated fabric consisting of deepseated (3000 m) structure representing a normal oceanic crust; 2) the northwestern zone with three seamounts elongated in the NW-SE direction (dredge stations NAN DR1, 2 at about 3500 m depth) and which represent the traces of a transform fault; 3) the southeastern zone with a seamount (dredge NAN DR3 and coring station KS 02 at about 3500 m and 2000 m depths respectively) which is part of the Scarborough Seamount chain (Fig. 1, 2); and 4) the eastern part of the China Sea ridge (east of the Scarborough seamounts) near the subduction zone of the Manila trench (dredge EST DR1, at about 3615 m depth). The subducting ridge shows *en échelon* normal faults parallel to the trench axis. The sedimentary cover on the ridge is very thin (less than 100 m) and the trench itself is devoid of thick sedimentary infill (Fig. 3, 4). On the island arc part, an accretional prism and fore arc basin were recognized from seismic refraction data (Lewis, Hayes, 1985). The trench floor between the subducting ridge and the inner trench wall is much narrower (about 500 m wide) than the area north and south of this collision zone.

Normal faults with vertical uplift of less than 100 m were observed near the base of the ridge (outer wall) at about 4000 m depth and on the upper part of the ridge at about 3300-3800 m depth (Fig. 2, 3, 4). These normal faults are a common feature on subducting oceanic plates. The curvature of the plate and the associated tectonic constraints give a maximum distension on the oceanic wall of a subduction zone. A dredge haul (EST DR1) placed on an escarpment above 3700 m enabled us to collect about 600 kg of vesiculated volcanics, hyaloclastites and a small amount of greenish gray pelagic sediment. This dredge is located at about 285 km east of the previous sampling sites (NAN DR3) in the Scarborough seamounts area (Fig. 1, 2). The coccoliths found in the hyaloclastites and on sediment coating the volcanics (EST DR1) belong to the late Miocene nannofossil zones CN7b and CN8a defined by Okada and Bukry (1980) corre-

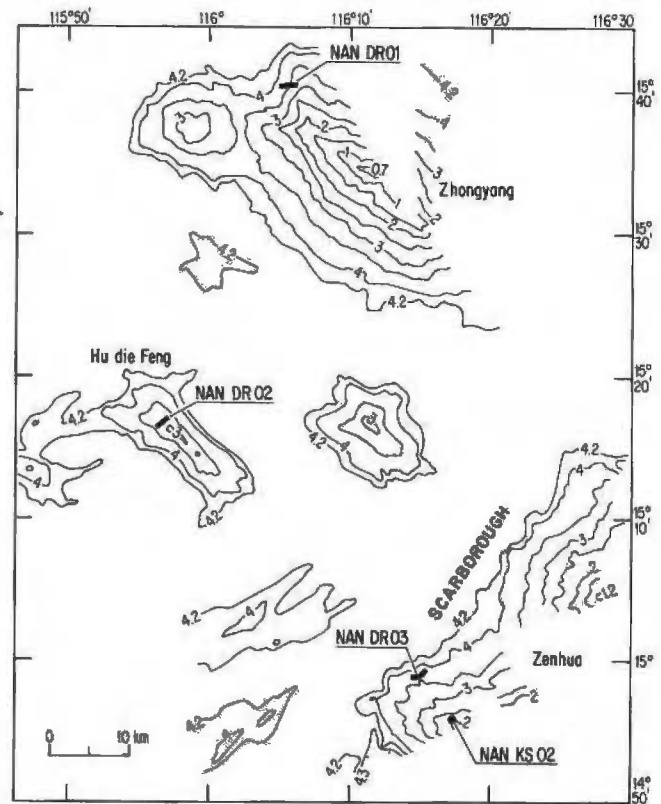


Figure 2

Bathymetric coverage (Seabeam) of the western portion of the South China Sea ridge showing the elongated and conjugated seamounts. The dredge hauls (NAN DR...) and the sediment coring (NAN KS02) sites carried out during the Nanhai cruise of the R/V Jean Charcot are shown.

sponding to an age of about 11 m.y. A core KS02 recovered near dredge haul Nan DR3 on a seamount located on the western flank of the Scarborough ridge contained pelagic sediment at contact with volcanics (Fig. 2). Dating the nannofossils of this core (KS02) was determined by C. Müller and gave an upper Miocene age (upper part of zone NN11 of Martini (1971) comparable to, but slightly younger than that obtained for the sample from the China Sea side of the Manila trench (NAN DR1, Fig. 2, 3).

## ANALYTICAL METHODS

Microprobe analyses of the glassy chilled margins were performed using a Camebax MBX instrument (Microsonde Ouest, Brest) by M. Bohn. Rare earth element distribution on the bulk rocks was determined by instrumental neutron activation analysis at the Centre Nucléaire de Saclay (CEA/CNRS). Major and trace element analyses of the bulk rocks were performed by atomic absorption method at the Geology Department of the Université de Bretagne Occidentale by J. Cotten (Tab. 1, 2). Some of the discrepancies observed between the glassy margin microprobe analyses and the bulk rock major element data reflect the degree of crystallinity (mineral accumulation), the occurrence of foreign inclusions (NAN DR1-2, NAN DR1-4) and the degree of rock alteration (NAN DR2-1, NAN DR1-2; Tab. 1, 2).

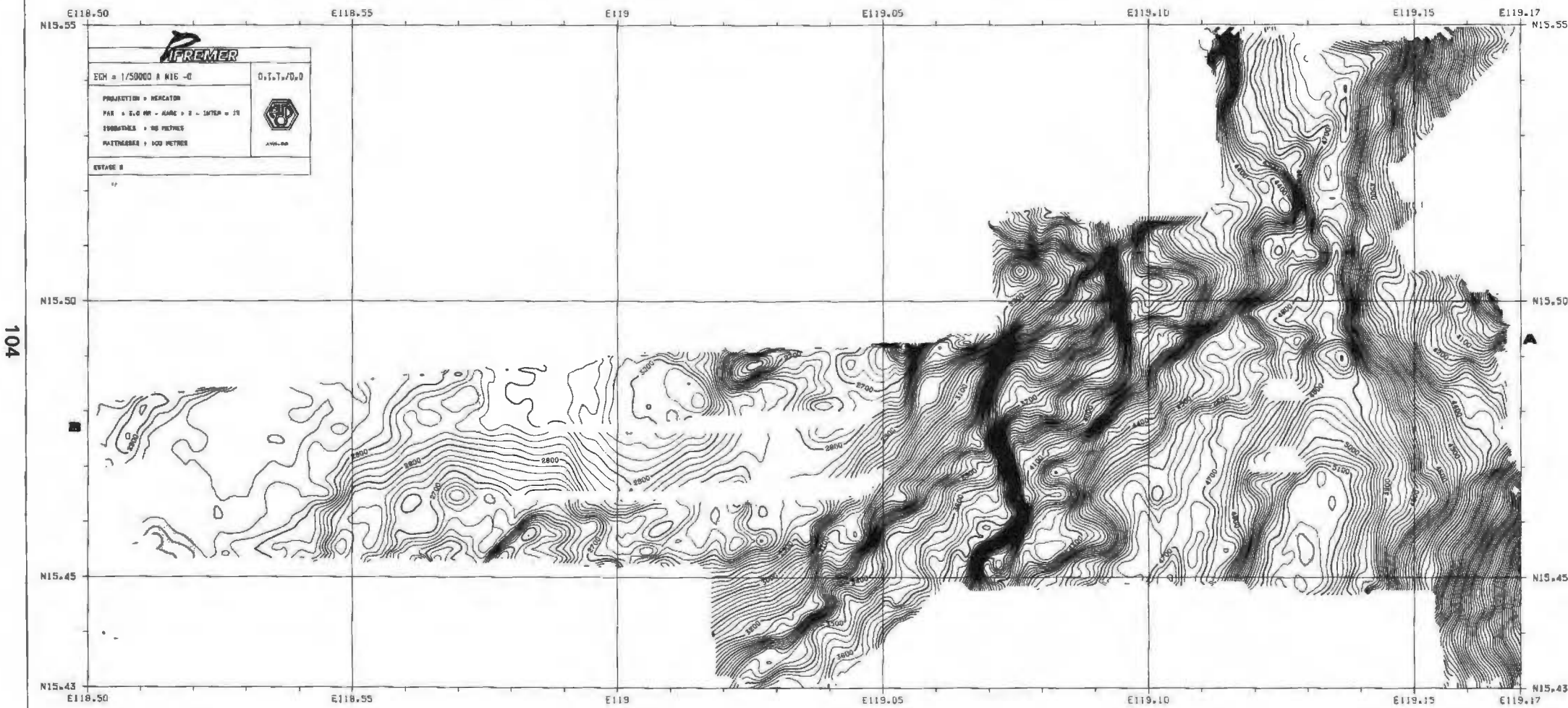


Figure 3  
Detailed Seabeam map of the Manila trench and its western oceanic wall. These data were acquired during the Estase cruise (1984). A-B indicates the swath of seismic reflection profile of Figure 4.

Table 1

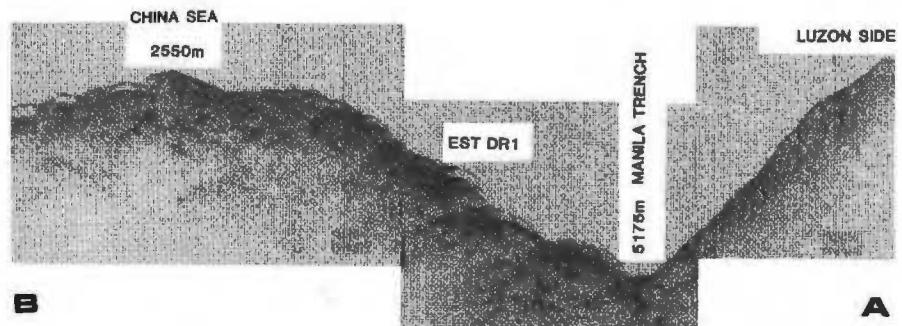
Microprobe analyses of glassy rocks dredged (DR...) from the Manila trench (ESTASE) and from seamounts of the China Sea basin (NANHAI). EST DR1 represents the average (3) analyses of several glass shards found in a hyaloclastite. Alk.-H.P.P.B. = alkali highly phyric plagioclase basalt, Alk.ol. = alkali olivine basalt.

	Alk.ol.basalt		Alk.-H.P.P.B.		Trachyte		Alk.ol.B.		Trachy basalt			
	EST DR1	EST DR1-1	EST DR1-2	EST DR1-3	EST DR1-4	EST DR1-7	NAN DR2-1	NAN DR1-3	NAN DR3-1	NAN DR1-4	NAN DR1-2	NAN DR1-7
SiO <sub>2</sub>	48.94	48.39	49.63	49.68	60.56	60.17	49.67	47.51	50.15	48.84	48.94	47.97
TiO <sub>2</sub>	2.73	2.74	3.22	3.21	1.12	1.16	2.65	3.05	2.79	2.95	2.79	2.77
Al <sub>2</sub> O <sub>3</sub>	17.45	17.12	14.43	14.96	16.52	16.83	15.83	16.71	17.40	17.20	17.40	17.09
FeO*	9.20	9.03	10.81	10.64	6.80	6.78	7.56	9.43	9.10	10.11	10.09	10.12
MnO	0.12	0.15	0.18	0.12	0.17	0.16	0.20	0.11	0.20	0.13	0.21	0.23
MgO	6.27	6.08	5.81	5.69	1.31	1.33	6.16	4.63	3.78	3.45	3.51	4.23
CaO	9.23	9.34	10.11	10.28	3.39	3.26	11.18	9.58	7.26	8.17	8.01	9.11
Na <sub>2</sub> O	3.18	3.09	2.59	3.03	2.82	2.42	2.81	2.93	4.03	3.21	3.62	3.39
K <sub>2</sub> O	1.45	1.42	1.28	1.39	3.32	3.24	2.24	2.28	3.06	2.72	2.90	2.20
P <sub>2</sub> O <sub>5</sub>	0.53	0.57	0.63	0.34	0.33	0.33	0.66	0.70	1.25	0.93	0.81	0.64
Total	99.10	97.93	98.69	99.34	96.34	95.68	98.96	96.93	99.02	97.71	98.28	97.75
CIPW-norms												
Q	—	—	0.87	—	19.33	21.87	—	—	—	—	—	0.05
or	8.58	8.40	7.57	8.22	19.64	19.16	13.25	13.49	18.10	16.09	17.15	13.01
ab	26.88	26.12	21.89	25.61	23.83	20.45	22.27	23.76	31.55	27.13	26.54	24.84
an	29.01	28.61	23.93	23.08	14.60	13.96	23.92	25.66	20.30	24.44	22.62	24.87
ne	—	—	—	—	—	—	0.80	0.54	1.36	—	2.20	2.07
lc	—	—	—	—	—	—	—	—	—	—	—	—
wo	5.62	5.90	9.22	10.74	—	—	11.44	7.28	3.20	4.17	4.95	6.75
di	3.37	3.50	5.05	5.95	—	—	7.29	3.96	1.59	1.91	2.22	3.28
fs	1.95	2.10	3.83	4.37	—	—	3.40	3.05	1.55	2.23	2.71	3.36
en	2.93	3.33	9.48	3.92	3.28	3.33	—	—	—	1.97	—	—
hy	—	—	—	—	—	—	—	—	—	—	—	—
fs	1.70	1.99	7.18	2.88	8.53	8.41	—	—	—	2.31	—	—
fo	6.56	5.86	—	3.05	—	—	5.68	5.33	5.50	3.32	4.59	5.11
ol	—	—	—	—	—	—	—	—	—	—	—	—
fa	4.21	3.88	—	2.47	—	—	2.92	4.53	5.93	4.29	6.18	5.77
mt	1.78	1.75	2.09	2.06	1.31	1.31	1.46	1.82	1.76	1.95	1.95	1.96
il	5.19	5.21	6.12	6.10	2.13	2.20	5.04	5.79	5.30	5.60	5.30	5.26
ap	1.25	1.35	1.49	0.80	0.78	0.78	1.56	1.66	2.96	2.20	1.92	1.51
C	—	—	—	—	2.92	4.21	—	—	—	—	—	—
Mg#	99.03	97.98	98.71	99.24	96.35	95.69	99.02	96.88	99.11	97.62	98.33	97.84
	58.60	58.30	52.75	52.62	28.58	28.95	62.86	50.49	46.31	41.48	41.94	46.47

FeO\* = total FeO estimated  $Fe_2O_3 = .133 \times FeO^*$  ( $Fe_2O_3 = .15 \times FeO$ , Brooks C. K., 1976).

Figure 4

Seismic reflection profile using a water gun (Sodera, 1.3 l) system showing a transect through the Manila trench and the ridge end. The location of dredge EST DR1 taken on the oceanic wall of the trench is shown.



## PETROLOGICAL DESCRIPTIONS

The rocks dredged from the China Sea seamounts and those from the Manila trench all belong to alkali-basalt-trachyte suites. Most of the samples are highly vesiculated and often irregularly shaped; a few show a slightly curved surface and faint radial jointing which is suggestive of pillow-lava forms. The dredged rocks from the Nanhai cruise (NANDR1, NANDR2 and NANDR3) all have abundant Fe-Mn coatings. A larger quantity of samples (about 100 kg) was obtained in the first dredge (NANDR1), located on the flank of the northern seamount near 15°50'N, while the other dredges (NANDR2 and NANDR3) contain only a few pieces (< 15 cm diameter) of Fe-Mn crust and vesiculated volcanics. The specimens showing curved

surface features sometime have thin (< 1 cm thick) glassy chilled margins suggesting that they are fragmented tubes and/or bulbous types of pillow flows. The dredge from the eastern part (EST DR1) contains about 600 kg of rocks of which a few samples are hyaloclastites. In addition there is one fragment of aphyric pillow lava flow (with radial jointing) mixed with highly vesiculated boulders of volcanics and scoriaceous fragments of trachytic rocks. Based on the texture, mineralogical variation and chemical composition of their glassy margins, the materials recovered are classified into six types:

- 1) alkali-olivine basalts;
- 2) alkali-olivine-plagioclase basalts;
- 3) highly phyric plagioclase (HPPB);
- 4) trachybasalt;
- 5) trachyte;
- 6) hyaloclastites.

Table 2

Bulk rock analyses of extrusive rocks from the Manila trench (EST DR...) and from the China Sea seamounts (NAN DR...). The analyses were done by Atomic Absorption method at the Université de Bretagne Occidentale by J. Cotten. Alk.Ol.Pl.B. = alkali olivine plagioclase basalt. Other symbols are the same as in Table 1. The trace element analyses done by neutron activation are included in parenthesis. I.L. indicates ignition loss at 70-1050°C. Because of their relative high normative "ne" content, the term basanite could also be used instead of trachybasalt, except for NAN DR3-1. Discrepancies between bulk rock and microprobe (glass) data are due to mineral accumulation (e.i. NAN DR2-1, cpx + ol; NAN DR1-4, Ti-mt).

	Alk.ol.B.		Alk.-H.P.P.B.		Trachyte		Trachy basalt		Alk.ol.Pl.B.		Alk.ol.B.		Trachy basalt	
	EST DR1-1	EST DR1-2	EST DR1-3	EST DR1-4	NAN DR1-1	NAN DR1-4	NAN DR1-5	NAN DR2-1 CRPG	NAN DR1-2 CRPG	NAN DR3-1 CRPG	NAN DR1-2 CRPG	NAN DR3-1 CRPG		
SiO <sub>2</sub>	47.20	48.30	49.25	58.30	44.90	44.20	46.00	43.48	40.11	48.51				
Al <sub>2</sub> O <sub>3</sub>	15.10	16.80	16.90	15.07	16.00	15.41	15.65	12.73	14.36	17.88				
F <sub>2</sub> O <sub>3</sub>	—	—	—	—	—	—	—	3.55	9.10	6.62				
FeO <sup>†</sup>	9.82	8.51	8.74	6.92	10.42	10.87	10.41	5.34	6.83	3.65				
MnO	.15	.14	.14	.21	.19	.19	.19	.17	1.58	.19				
MgO	8.23	4.95	4.99	1.33	6.86	6.70	6.97	9.96	5.8	2.14				
CaO	9.02	11.60	11.06	3.63	10.10	9.75	10.19	9.38	8.8	7.94				
Na <sub>2</sub> O	3.26	3.10	2.97	5.55	3.36	3.92	3.46	2.81	3.14	4.11				
K <sub>2</sub> O	1.24	1.11	1.06	3.77	1.73	2.05	1.68	2.05	1.64	2.89				
TiO <sub>2</sub>	2.22	2.20	2.29	1.02	2.21	1.86	2.21	2.10	2.97	2.41				
P <sub>2</sub> O <sub>5</sub>	.50	.55	.40	.45	.50	.50	.50	.36	.60	1.17				
I.L.	.67	1.60	1.09	2.40	2.27	1.59	1.46	6.16	3.41	1.89				
H <sub>2</sub> O <sup>-</sup>	.65	.51	.38	.09	.20	.36	.28	—	—	—				
Total	97.41	98.86	98.83	98.65	98.57	97.04	98.72	98.09	98.34	99.40				
CIPW-norms														
Q	—	—	—	1.26	—	—	—	—	—	—				
or	7.33	6.57	6.27	22.30	10.23	12.13	9.94	12.13	9.70	17.09				
ab	25.22	25.63	25.10	46.91	13.63	9.02	15.72	12.64	16.69	34.38				
an	22.87	28.61	29.61	5.04	23.43	18.36	22.17	16.03	20.21	21.76				
ne	1.26	0.31	—	—	8.01	13.07	7.33	6.02	5.34	0.19				
lc	—	—	—	—	—	—	—	—	—	—				
wo	7.75	10.58	9.51	4.14	9.75	11.14	10.46	11.81	8.17	4.24				
di	4.74	5.89	5.27	1.18	5.47	5.99	5.91	9.15	6.08	5.52				
fs	2.56	4.27	3.87	3.16	3.88	4.78	4.11	1.36	1.28	2.47				
en	—	—	4.21	2.15	—	—	—	—	—	—				
hy	—	—	—	—	—	—	—	—	—	—				
fs	—	—	3.09	5.78	—	—	—	—	—	—				
fo	11.09	4.54	2.10	—	8.09	7.53	8.06	11.03	5.90	0.12				
ol	—	—	—	—	—	—	—	—	—	—				
fa	6.63	3.62	1.70	—	6.33	6.63	6.18	1.81	1.37	0.06				
mt	1.90	1.64	1.69	1.34	2.01	2.10	2.01	5.15	13.20	9.60				
il	4.22	4.18	4.35	1.94	4.26	3.53	4.20	3.99	5.64	4.58				
ap	1.18	1.30	0.95	1.06	1.18	1.18	1.18	0.85	1.42	2.77				
C	—	—	—	—	—	—	—	—	—	—				
(ppm)														
Rb	35	22 (20)	22 (30)	106 (85)	40 (31)	46	38 (44)	(36)	(42)	(63)				
Sr	442	415	400	325	685	618	624	—	—	—				
Ba	315 (363)	240 (469)	200 (345)	1215 (1312)	475 (411)	369 (407)	420 (422)	(131)	(385)	(623)				
V	210	240	230	≤20	210	195	215	—	—	—				
Cr	(371)	138 (103)	119 (116)	≤10 (39)	240 (200)	249 (246)	263 (184)	(458)	(212)	(60)				
Co	43 (50)	31 (25)	33 (29)	3 (3)	40 (37)	39 (40)	42 (43)	(36)	(34)	(41)				
Ni	178	51	54	4	96	97	102	—	—	—				
Cu	57	154	75	10	71	68	61	—	—	—				
Sc	25	24.8	24.3	12	24.5	21.9	25.6	27	20.7	11.7				
Hf	4.8	3.7	3.8	11	4.9	5.1	5.0	5.5	4.6	7.2				
Th	4.8	3.1	3.3	11.7	6.1	6.7	6.3	6.6	6.2	8.9				

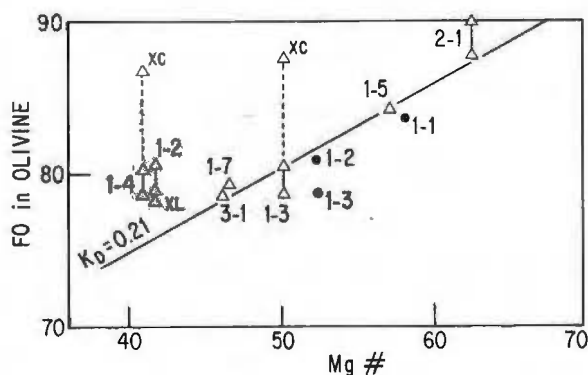


Figure 5  
Mg# and forsterite content of olivine.  $K_D$  is the distribution coefficient of the microphenocrysts and phenocrysts of olivine. The empty triangles are samples from the Nanhai cruise in the China basin (seamounts area). The black dots are the volcanics from the Manila trench. Xc = xenocrysts and Xl = xenoliths.

### Alkali olivine basalts

They are represented by samples NAN DR2-1 and EST DR1-1. They consist essentially of early formed Mg-rich olivine ( $Fo_{83-90}$ ) and reddish brown euhedral chrome-spinel (Tab. 1, 2, 3). They are deprived of early formed clinopyroxene and the plagioclase content (EST DR1-1) is less prominent than in the other basalts. The texture of these rocks is semi-fluidal to glomeroporphyritic due the agglomeration of olivine crystals (NAN DR2-1). The most crystalline interior of the samples shows late plagioclase microlites (EST DR1-1) with  $an_{69}$  (Tab. 4). The main difference between these two samples is that NAN DR2-1 has a higher content of olivine phenocrysts (5-6%) with a higher forsterite content ( $Fo_{87-90}$ ). In addition, these

samples are characterized by a relatively high Mg# (atomic proportion  $Mg^{2+}/(Mg^{2+} + Fe^{2+})$ ) of about 58-63 (Tab. 1, Fig. 5).

**Alkali olivine plagioclase basalts** (NAN DR1-3, DR1-5 and DR1-6)

They differ from the previous sample by a generally lower content in forsterite ( $Fe_{0.83-0.84}$ ) of their olivine. Since these latter samples (DR1-5 and DR1-6) are deprived of glassy margins, only whole rock analyses are available (Tab. 2). On this basis, despite alteration, they are tentatively classified as being intermediate volcanics between the least evolved alkali olivine basalt (*i. e.* EST DR1-1) and the trachybasalts (NAN DR1-1, NAN DR1-3, NAN DR3-1). We should, however,

point out that their bulk analyses are strongly influenced by the presence of fair amount (3-5%) large xenocryst material.

**Highly pyritic plagioclase basalts (HPPB)** (EST DR1-3, EST DR1-2)

They consist of early formed plagioclase (> 15%) megacrysts, phenocrysts and microphenocrysts set in a groundmass of plagioclase microlites and dark mesostasis. Olivine phenocrysts and xenocrysts of clinopyroxene with a corona texture are occasionally seen. Augitic clinopyroxene microphenocrysts are also observed (NAN DR1-3). The early formed plagioclase are characterized by lower orthoclase content (< 1%) than that found in the other rock types (> 1,0%; Tab. 1, 4).

Table 3

Microprobe analyses of olivine from glassy margins of rocks collected in the Manila trench (ESTASE) and in the China Sea basin (NANHAI).

	EST 1-1	EST 1-2	EST 1-3	EST DR1	NAN 1-3	NAN 1-2	NAN 1-4	NAN 1-1	NAN 2-1	NAN 3-1
SiO <sub>2</sub>	40.36	39.21	39.06	39.37	39.37	39.25	39.77	39.47	40.89	38.92
FeO*	15.62	18.22	19.75	18.88	17.99	17.70	18.51	17.75	9.47	19.47
MnO	0.19	0.33	0.30	0.12	0.30	0.20	0.18	0.30	0.17	0.34
MgO	45.46	43.94	41.64	42.62	42.37	42.32	43.13	42.84	* 49.18	41.12
CaO	0.25	0.27	0.25	0.26	0.29	0.46	0.26	0.22	0.31	0.16
Total	101.88	101.97	101.00	101.25	100.32	99.93	101.85	100.58	100.02	100.01
Fo	83.67	80.84	78.72	79.99	80.51	80.82	80.42	80.87	90.09	78.78

Table 4

Microprobe analyses of early formed plagioclase and anorthoclase (Anrth.) from the Manila trench (DR1...) and from the China Sea basin seamounts (NANHAI). (XC) indicates a large xenocryst of zoned andesine (and.) olig. = oligoclase.

	1-1	1-3	DR1	1-4 And.	1-4 Olig.	1-13 Anrth.	NAN 1-3	NAN 1-2	NAN 1-4	NAN 3-1	NAN 3-1XC
SiO <sub>2</sub>	50.19	49.19	50.70	58.24	61.43	64.60	50.50	51.75	54.07	52.36	56.16
Al <sub>2</sub> O <sub>3</sub>	30.91	31.93	30.35	27.17	23.00	21.02	30.88	30.40	28.44	30.05	27.47
FeO	0.78	0.48	0.58	0.35	0.09	0.16	0.68	0.59	0.23	0.56	0.28
MgO	0.24	0.15	0.19	0.02	0.02	0.00	0.14	0.10	0.05	0.12	0.00
CaO	13.98	15.19	13.90	8.46	3.83	1.75	14.22	12.74	10.65	12.62	9.53
Na <sub>2</sub> O	3.37	2.68	3.41	5.92	7.90	7.24	3.35	3.95	5.09	4.13	5.71
K <sub>2</sub> O	0.25	0.16	0.17	0.08	1.83	5.37	0.21	0.28	0.13	0.40	0.67
P <sub>2</sub> O <sub>5</sub>	—	—	0.04	0.08	0.03	0.02	—	0.10	—	0.10	0.08
Total	99.71	99.79	99.33	100.80	98.13	100.16	99.96	99.91	98.66	100.34	99.90
ab	29.92	23.95	30.45	53.96	70.41	60.63	29.55	35.31	46.00	36.33	50.01
or	1.44	0.94	0.98	3.37	10.74	30.14	1.24	1.63	0.79	2.29	3.86
an	68.64	75.11	68.57	42.67	18.85	8.23	69.21	63.07	53.21	61.38	46.13

Table 5

Microprobe analyses of clinopyroxene from rocks dredged from the Manila trench (ESTASE) and from the China Sea seamounts (NANHAI). Phn. = phenocrysts; Mph. = microphenocrysts.

	Trachy basalt							Alk. ol.Pl. Basalt NAN 1-7 Mph.	Alk.ol. Basalt NAN 2-1 Phn.
	EST 1-3 Phn.	EST 1-4 Phn.	NAN 1-2 Phn.	NAN 1-3 Phn.	NAN 1-4 Phn.	NAN 3-1 Mph.	NAN 1-7 Mph.		
SiO <sub>2</sub>	52.59	51.14	47.02	45.35	47.73	45.77	46.99	48.32	52.14
Al <sub>2</sub> O <sub>3</sub>	2.42	1.46	9.55	8.67	7.90	9.54	9.28	5.78	2.63
FeO	7.03	14.96	6.90	6.26	7.36	7.39	6.83	6.94	4.23
MnO	0.12	0.79	0.21	0.13	0.06	0.11	0.09	0.04	0.17
MgO	16.51	11.26	12.66	13.05	12.97	12.82	12.93	14.15	17.13
CaO	20.36	19.71	21.38	21.22	21.24	20.18	21.62	21.99	21.73
Na <sub>2</sub> O	0.34	0.38	0.60	0.50	0.61	0.63	0.58	0.49	0.25
TiO <sub>2</sub>	1.08	0.51	2.12	2.89	2.13	2.87	2.02	1.78	0.86
Cr <sub>2</sub> O <sub>3</sub>	0.31	0.00	0.03	0.30	0.00	0.31	0.00	0.37	0.69
Total	100.45	100.21	100.49	98.37	100.00	99.63	100.34	99.93	99.83
wo	41.63	41.34	46.78	47.71	47.14	45.98	48.05	46.66	44.40
en	46.96	32.82	40.30	41.02	39.97	40.66	39.96	41.78	48.70
fs	11.41	25.84	12.92	11.27	12.90	13.36	12.00	11.56	6.90

### Trachybasalts

They are represented by samples NAN DR1-2, NAN DR1-1, NAN DR1-3, NAN DR1-4, NAN DR3-1. They consist essentially of early formed olivine, clinopyroxene and plagioclase. The amount of clinopyroxene (> 1%) is higher than that of the other rock types. Sample NAN DR1-1 does not have a glassy chilled margin and only bulk chemical data is available (Tab. 1, 2). The term trachybasalt is used here because of the semi-fluidal textural features observed where microlites of plagioclase and the vesicles are arranged in a sub-parallel fashion. However, because of their relatively high normative nepheline (6-13%) and low SiO<sub>2</sub> (< 45%) content, these rocks could also be called basanites, except for sample NAN DR3-1. These samples are also characterized by a low Mg# (41-47) and the forsterite content of their olivine (Fo<sub>80</sub>; Tab. 1, 2, 3). They differ from the alkali olivine basalts by their higher normative orthoclase and nepheline content (Tab. 1, 2). Often the clinopyroxene shows zoning and its average composition is that of a salite (en<sub>40</sub>fs<sub>12</sub>) (Fig. 7; Tab. 5).

### Trachyte

It was only found in one dredge haul (EST DR1-4) near the Manila trench. This dark-grey colored rock has a black "pumice like" appearance with flow textural features due to the parallel arrangement of the vesicles and the plagioclase (oligoclase) set in a mineral-crowded glassy matrix. The orthoclase content of the feldspar varies between 3% among the microlites up to 9% for the phenocrysts. The composition of the augitic clinopyroxene in this rock is more Fe enriched than that of all the other analysed samples, and is found in phenocrysts (< 1%; Fig. 6, 7, Tab. 5). Scarce apatite micro-phenocrysts were found scattered in the glassy matrix. The apatites are believed to be primary because of their euhedral texture and the absence of any other

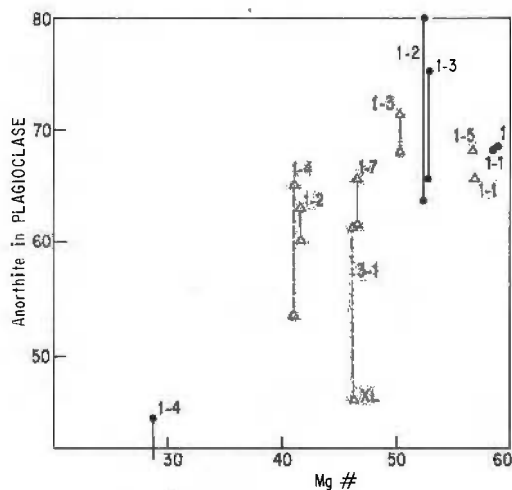


Figure 6  
Mg# versus anorthite content of plagioclase. The dotted and the continuous tielines between samples indicate mineral analyses from the same specimen. The continuous lines show composition of matrix and phenocryst (enriched in an). The dotted lines indicate xenoliths found in the host rock.

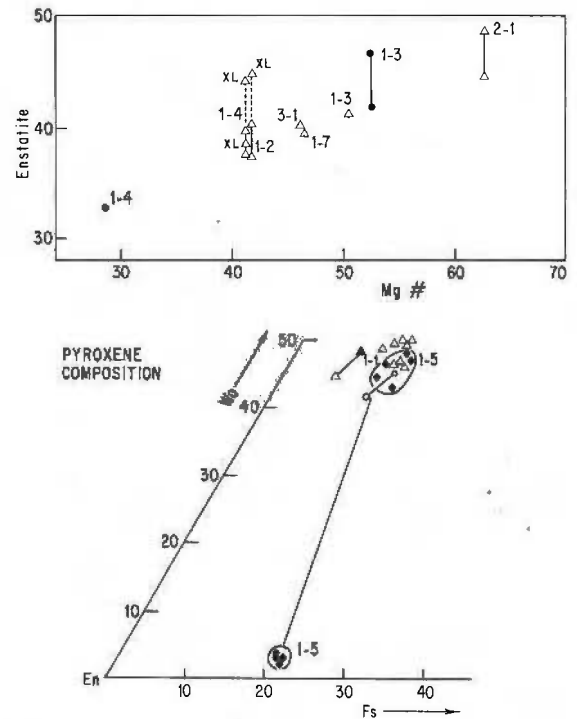


Figure 7

Clinopyroxene variation diagrams. Mg# versus Enstatite content of clinopyroxene. The symbols are the same as in Figure 4. The triangular diagrams (en-wo-fs) show the composition of clinopyroxene and orthopyroxene xenoliths (black diamonds) found in the same rock (NAN DR1-5). The tie line between signs indicates the range in compositional variation between matrix and phenocryst clinopyroxene. The empty circles are a dredge haul (EST DR1) from the Manila trench. The others are from the China basin seamounts.

signs of secondary mineral precipitates in the fresh glassy trachyte. A few phenocrysts of sodic plagioclase and anorthoclase were also found (Fig. 6 and Tab. 4). Some of the larger plagioclase show a mirmekitic texture due to glass inclusions.

### Hyaloclastites

Among the several samples recovered, two were studied in detail (EST DR1 and NAN DR1-7). They consist of highly vesiculated glassy shards with a pilotaxitic and hypohyaline texture and abundant dark mesostasis and haphazard arrangements of tiny plagioclase microlites. The glassy shards in samples NAN DR1-7 appear to be more homogeneous and are essentially made up of olivine and plagioclase phenocrysts in glass with fluidal texture. The shards forming the hyaloclastites are cemented together by Fe-Mn hydroxide intermixed with pelagic sediment. From chemical analyses performed on several shards from each specimen, it was observed that they have a homogeneous composition, and they are believed to have been derived from the same type of rocks as those associated in the dredge hauls. Because of their small size and the limited amount of their early formed phases it is difficult to classify hyaloclastites in relation to the alkali basalt suites. However, on the basis of their chemistry expressed in terms of their Mg# it is observed that sample NAN DR1-7 is closer in composition to that of the trachybasalt (Tab. 1) while sample EST DR1 with a Mg# of 58 is rather similar in composition to the alkali olivine basalt (Tab. 1).

Table 6

Microprobe analyses of chrome spinel (Cr. Spn), hercynite (Grn. Sp), Ti-magnetite (Ti-Mt) and ilmenite (Ilm) found in rocks from the Manila Trench (ESTASE) and from the China Sea seamounts (NANHAI). (Ilm.XI) indicates ilmenite included in a xenolith.

	EST 1-1 Cr.Spn	EST 1-4 Ti.Mt	EST 1-4 Ilm	NAN 1-2 Grn.Sp	NAN 1-3 Cr.Spn	NAN 2-1 Cr.Spn	NAN 1-5 Ilm.XI
SiO <sub>2</sub>	0.50	2.62	1.99	0.04	0.20	0.16	0.00
Al <sub>2</sub> O <sub>3</sub>	28.92	4.13	1.14	49.65	30.99	26.10	0.88
FeO	17.80	37.79	35.26	19.70	12.71	14.05	31.96
Fe <sub>2</sub> O <sub>3</sub>	15.49	38.46	11.89	8.61	8.11	9.14	5.80
MnO	0.18	0.77	0.92	0.21	0.18	0.21	0.30
MgO	13.94	2.17	3.30	13.65	16.44	15.04	8.44
CaO	0.12	0.12	0.13	0.00	0.02	0.10	0.00
TiO <sub>2</sub>	3.02	12.35	45.88	0.85	1.18	1.57	51.92
Cr <sub>2</sub> O <sub>3</sub>	21.24	0.00	0.03	8.31	30.86	33.30	0.05
Total	101.22	98.56	100.58	101.10	100.69	99.73	99.31

## FOREIGN INCLUSIONS

The foreign inclusions consist of the xenoliths and xenocrysts which occur in the evolved alkali basalt suites such as the trachybasalts (NANDR1-3, NANDR1-4, NANDR1-2, NANDR1-1, NANDR3-1) and the alkali olivine-plagioclase basalts (NANDR1-5, NANDR1-6). While the xenoliths are easily distinguished, the xenocrystal phases are more difficult to differentiate from the phenocrysts.

Among the xenoliths found in the alkali basalts (NANDR1-1, DR1-5, DR1-2) and in the trachybasalts, clinopyroxene is the most abundant constituent (about 85%), while orthopyroxene (5-7%) and the olivine (5%) are less prominent. The opaques and dark-green aluminous spinel comprise less than 2% of the bulk xenolith content. These mineral associations correspond to an olivine-websterite composition. One small (< 5 mm diameter) xenolith containing plagioclase and clinopyroxene was found in a sample of trachybasalt (NANDR3-1).

From their appearance, the xenoliths are divided into: 1) one with a granulated texture (NANDR1-5); and 2) several with allotriomorphic granular texture (NANDR1-1, NANDR3-1). The size of these round xenoliths varies between 0.2 cm and 1.2 cm in diameter. Individual grain size is about 100-800 microns in diameter. The clinopyroxene shows a strong undulatory extinction and kink band type of deformation. The larger clinopyroxene shows the presence of granulated material made up of the same mineral (DR1-5). The boundaries between the uncrushed pyroxenes are irregular and often interlocking. Traces of interstitial crystallization of plagioclase (an<sub>62</sub>), olivine (Fo<sub>80</sub>), titanomagnetite and aluminous spinel (hercynite), with a composition similar to that of the host rock (NANDR1-1, NANDR1-5) occur.

All the phases encountered in the xenoliths are homogeneous in composition. The olivine is the only phase which is particularly altered into a reddish brown Fe-hydroxysilicate and its forsterite content is Fo<sub>77-79</sub> (Tab. 7). The clinopyroxene is an augite salite type

Table 7

Microprobe analyses of olivine and clinopyroxene xenocrysts (XNCR) and xenoliths (XNL) from the China Sea Seamounts (NANHAI cruise).

Wt%	DR1 XNL	DR1-1 XNCR	DR1-2 XNL	DR1-3 XNCR	DR1-4 XNCR
SiO <sub>2</sub>	38.62	40.44	39.08	40.64	40.50
FeO	21.18	13.68	19.64	11.90	12.27
MnO	.17	.24	.15	.14	.19
MgO	40.55	46.49	41.33	47.65	46.91
CaO	.11	.16	.09	.27	.20
Total	100.62	100.91	100.37	100.60	100.07
Fo	77.2	85.712	78.82	87.53	86.98
Wt%	DR1-1 CPX XNL	DR1-1 OPX XNL	DR1-2 CPX XNCR	DR1-4 CPX XNCR	DR1-5 CPX XNL
SiO <sub>2</sub>	47.50	52.19	49.84	48.83	46.42
TiO <sub>2</sub>	1.78	.38	.82	1.02	2.19
Al <sub>2</sub> O <sub>3</sub>	8.22	5.37	6.19	7.81	10.11
FeO	6.84	13.39	6.50	6.51	7.77
MnO	.03	.19	.02	.01	.11
MgO	13.21	28.30	14.60	14.28	12.17
CaO	20.37	.85	19.82	19.64	20.93
Na <sub>2</sub> O	.58	.02	.77	.78	.71
Cr <sub>2</sub> O <sub>3</sub>	.13	.11	.30	.57	.05
Total	98.67	100.80	98.83	99.45	100.47
Wo	46.19	1.68	43.14	44.04	47.57
Cn	41.64	77.46	44.87	44.55	38.47
fs	12.17	20.86	11.30	11.41	13.46

enriched in  $\text{Al}_2\text{O}_3$  (8-10%) (Tab. 7) and is associated with a Ca-poor orthopyroxene ( $\text{wo}_{1.7}\text{en}_{77.4}\text{fs}_{20.9}$ ). The bottle-green and opaque aluminous spinels found in the xenoliths and also in the form of individual large (0.5 mm diameter) resorbed crystals within the host rock are deprived in  $\text{Cr}_2\text{O}_3$  content ( $< 20\%$ ) in comparison with the reddish brown euhedral chrome-spinel found in the least evolved alkali-olivine basalts (NAN DR1-1 and NAN DR2-1). Granules of ilmenite are also found in these xenoliths (Tab. 6).

*Clinopyroxene xenocrysts* are recognized by their undulatory extinction and their resorbed nature, and have a slightly higher enstatite content ( $\text{en}_{4.5}\text{Fs}_{1.1}$ ) and a lower  $\text{TiO}_2$  content (1.5%; NAN DR1-2, NAN DR1-4) than those of the xenoliths (Tab. 7). They are closer in composition to the pyroxene phenocrysts and micro-lites of the least evolved olivine alkali basalt (NAN DR2-1; Tab. 7, Fig. 7). The clinopyroxene are surrounded by reaction rims (corona structure) of a Mg-depleted pyroxene ( $\text{en}_{3.7}\text{Fs}_{1.4}$ ) relatively rich in  $\text{TiO}_2$  ( $> 2\%$ ; *i.e.* NAN DR1-2; Tab. 7, Fig. 7). This is due to the reequilibration of the xenocrysts with the melt in which they were trapped, and should not be confused with the zoning effect that some pyroxenes show. In fact, the composition of the pyroxene rims is comparable to that of the late formed phases found in the matrix of the host rock.

*Olivine xenocrysts* also show a more Mg-rich composition ( $\text{Fo}_{85-88}$ ) than that found in the xenoliths (Tab. 7, Fig. 5). The Mg-rich olivine (NAN DR1-1, DR1-3, NAN DR1-4) consists of partially resorbed crystals; some corona structures due to the presence of more Fe-rich olivine rims have the composition ( $\text{Fo}_{79-80}$ ) of that found in equilibrium with the melt (NAN DR1-3). Myrmekitic texture showing "worm-like" inclusions of the cryptocrystalline matrix is sometimes seen in the larger xenocrysts (EST DR3-7).

*Plagioclase xenocrysts* (up to 1 cm diameter) were found in samples NAN DR1-6 and NAN DR3-7. These plagioclase xenoliths are characterized by reverse zoning with a sodic core ( $\text{an}_{4.6}\text{an}_{5.8}$ ) corresponding to a calcic andesine and a more calcic rim ( $\text{an}_{6.1}$ ) having the composition of the plagioclase of the host rock. They differ from megacrysts by their scarcity (few grains in each specimen) and by their resorbed textural features.

#### Significance of the foreign inclusions

The granulated fabric observed of the xenolith found in sample NAN DR1-5 does not show any preferential orientation for the grains, and the only intercumulus material is represented by the dark green Mg-Al spinel, plagioclase and olivine. Because of their limited extent and the rarity of grain deformation, it is concluded that these xenoliths represent tectonized upper mantle material. However, we believe that the granulated texture resulted from local crustal fracturing and magmatic reequilibration during their ascent to the surface. The seamont from which this particular sample (NAN DR1-5) was taken is located roughly on a NW-SE linear tectonic feature which might correspond to a major fracture zone (Pautot *et al.*, 1986). The pre-

sence of Ti-poor ( $\text{TiO}_2 < 1\%$ ) and Ti-rich orth- and clinopyroxene in some specimens (NAN DR1-2, NAN DR1-1) suggest that they represent crystal fractionated products from both tholeiitic and alkali basalt magmas. Also the heterogeneous composition of the other foreign inclusions, such as the occurrence of sodic plagioclase (andesine) and sodic labradorite (NAN DR1-6, NAN DR3-1) comparable to that found in the most evolved sample (trachyte) suggests a magmatic crustal accumulation from earlier melts. Differentiation by crystal fractionation at shallow depth in the crust is suggested by the presence of both Mg-rich ( $\text{Fo}_{85-88}$ ) and Mg-poor ( $\text{Fo}_{77-79}$ ) olivine xenoliths and xenocrysts within the same alkali basalt host (NAN DR1-1; Tab. 2, 7). In addition, both the Mg-rich olivines found in the most evolved trachybasalt (NAN DR1-4, NAN DR1-2) are comparable to the magmatic olivine found in the least evolved olivine alkali basalts (NAN DR2-1; Tab. 3, 7, Fig. 5). It is likely that the foreign inclusions brought to the surface by the host alkali basalt suites represent at least three different crustal zones existing beneath the seamounts from the China Sea: 1) a websterite zone; 2) a Mg-rich olivine bearing zone (perhaps of dunitic composition); and 3) a gabbroic zone. In addition, the occurrence of Na-plagioclase ( $\text{an}_{46}$ ) (NAN DR1-6) indicates that a more evolved fractionated zone might exist beneath the seamount. However because of the scarcity, the dispersed nature and the size (0.5-10 mm diameter) of these foreign inclusions, it is difficult to make further speculation on their origin.

#### DEGREE OF ROCK ALTERATION

The samples collected from the Scarborough Seamount area (NAN DR 3) and further north (DR 1, DR 2) are among the most altered ones. They are characterized by a thick (0.5-2 cm) Fe-Mn coating. When glassy margins are present they are partially altered into a thick palagonite crust (1-0.5 m thick). Many of the vesicles are also filled with calcite and Fe-hydroxide products. The mineral alteration is essentially expressed by the presence of reddish brown Fe-Al-Mg hydrated silicate phases forming reaction rims around phenocrysts and microphenocrysts of olivine (NAN DR1-2, NAN DR1-4, NAN DR1-5 and NAN DR1-6), while the olivine in the xenoliths are less affected by secondary alteration effects. In one case (NAN DR3-1), most of the early and late-formed olivines are completely replaced by deuteric alteration products. This is also expressed by a higher ferric ferrous ratio ( $\text{Fe}_2\text{O}_3/\text{FeO}=1.66$ ) when compared with some other basalts (NAN DR1-2, NAN DR2-1) having a  $\text{Fe}_2\text{O}_3/\text{FeO}$  ratio of less than 1. Veinlets of Fe hydroxides and palagonite occur in several glassy margins of these samples (NAN DR1-2, NAN DR2-1), and their ignition loss is higher (3-6%) than that of other basaltic rocks (Tab. 2).

The dredge haul from the subducting wall of the Manila Trench (EST DR1) contains rock samples which are generally less affected by alteration when compared

with the samples from the western part. The freshest specimens are represented by the pillow lava fragments (EST DR1-1) and the trachytes (EST DR1-4). The HPPB are also relatively fresh and both olivine and plagioclase megacrysts are intact. The ignition loss of these rocks generally ranges between 1 and 2% (Tab. 2). The alkali olivine basalt (pillow lava fragment, EST DR1-1) has the lowest ignition loss (0.67%) while the trachyte (EST DR1-4) reaches up to 2.40% (Tab. 2). It is believed that these values of ignition loss are representative of the original volatile content of the respective melts because such values are found for fresh rock of similar composition. The freshest portion of the samples were chosen in order to perform bulk rock analyses.

### MINERALOGICAL VARIATIONS

The extent of compositional variation between the various rock types is consistent with the change in composition of the mineral phases. The variability trends of the major mineral phases is best visualized with respect to the Mg# of their corresponding glassy matrix (Fig. 4, 5, 6).

*Clinopyroxene* is one of the commonest minerals encountered and is found as phenocrysts, microphenocryst and matrix constituents. The rims of pyroxene are often altered into a reddish brown product comparable to that of olivine. Most of the clinopyroxene are salites with a TiO<sub>2</sub> content higher than 2% except for that found in the least evolved olivine alkali basalt (NAN DR2-1) and in the trachyte (EST DR1-4) where diopsidic (en<sub>44-48</sub>fs<sub>6-7</sub>) and augitic (en<sub>33</sub>fs<sub>26</sub>) pyroxene occur respectively (Tab. 5; Fig. 6, 7). The field of clinopyroxene composition overlaps that of the xenoliths and xenocrysts, which have a tendency to be less rich in TiO<sub>2</sub> (< 2%). The alumina content follows that of the titania; that is, the lower Al<sub>2</sub>O<sub>3</sub> (< 5.2%) are found among the diopsidic and augitic clinopyroxene (NAN DR2-1; EST DR1-4). The compositional range between early and late formed clinopyroxene is small and is mainly due to a depletion in the molecular content of wollastonite (< 5%) in the phenocrystal phases.

*Plagioclase* varies in composition between andesine (an<sub>44</sub>) and bytownite (an<sub>80</sub>). Megacrysts (> 0.4 mm up to 10 mm in length), phenocrysts (0.1-0.4 mm), microphenocrysts (0.05-0.2 mm in length) and microlites (< 0.05 mm in length) are found abundantly. There is a good correlation between the late-formed plagioclase phases and the melt composition as expressed by the change in anorthite content with the Mg# characterizing the various rock types (Fig. 6). The most calcic plagioclases (bytownite) are found in the HPPB (play-rich basalts) (Tab. 4). It is believed that these megacrysts are not foreign inclusions because they are homogeneously distributed within the specimens, do not form clusters or aggregates with other mineral phases, and lack distinct reverse zoning. Instead, they are believed to be the result of abnormal plagioclase accumulation during magmatic segregation prior to eruption.

*K-Na feldspars* with a texture (quadrille) and habit

(tabular) of anorthoclase were found in a trachyte (EST DR1-4). Discontinuous joints and albite twinning are prominent in the phenocrysts, while the microlites have a texture comparable to the other plagioclase laths (albite twins). They differ from the plagioclase by their higher K<sub>2</sub>O content (> 1.4%; Tab. 4). There is a difference in K<sub>2</sub>O content between that of the phenocrysts (< 1.8%) and that of the microlite (2-4%; Tab. 4). *Olivine* is usually found as euhedral, phenocrystal, microphenocrystal and microlite phases among all the samples with the exception of the most evolved trachyte. Olivine is rarely zoned; it occurs in the form of isolated crystals, in agglomeration with plagioclase and/or other olivines, and is rarely associated with clinopyroxene except in the xenoliths. The trend of olivine variability between the various rock types is considerable (Fo<sub>90</sub> et Fo<sub>79</sub>) when compared to that occurring in the same samples (Fig. 4). Indeed, within individual samples there is a small difference in composition between the early and late formed olivine (< Fo<sub>83</sub>; Fig. 5, Tab. 3). The distribution coefficient of Fe and Mg between the liquid and the olivine is about 0.21-0.25, while for the xenocrystal phase the K<sub>D</sub> value is much lower (< .17; Fig. 4).

*Opaques* consist of titanomagnetite, ilmenite and spinel. They occur either as early or late formed mineral phases except for some varieties of spinel. Among the spinels two varieties are observed: 1) a reddish, light-brown Cr-spinel enriched in Cr<sub>2</sub>O<sub>3</sub> (21-34%) found as small euhedral crystals associated with Mg-rich olivine in the least evolved sampled (NAN DR2-1, EST DR1-1 and NAN DR1-3); and 2) a dark-green spinel enriched in Al<sub>2</sub>O<sub>3</sub> (50-60%) and in MgO (13-14%) and depleted in Cr<sub>2</sub>O<sub>3</sub> (< 10%) when compared to the reddish-brown spinel (Tab. 6). The dark-green spinel is a hercynite, it occurs as large-sized (up to 1-2 mm diameter) and resorbed crystals, but it is also found as a matrix constituent in the most evolved type of basaltic rocks. Early-formed ilmenite is found in the trachytes (EST DR1-4, DR1-13) while titanomagnetite is more prominent in the less evolved alkali basalt suites (Tab. 6).

### CRYSTAL CHEMISTRY AND TRACE ELEMENT VARIATIONS

Much of the chemical variation observed among the various basaltic suites is the reflection of their mineral distribution. The TiO<sub>2</sub> and the P<sub>2</sub>O<sub>5</sub> content of the alkali basalt suites are mainly affected by the crystallization of titanomagnetite, ilmenite and apatite. The depletion in P<sub>2</sub>O<sub>5</sub> (< 50%) content of the trachyte (EST DR1-4) is probably due to the crystallisation of apatite. The maximum P<sub>2</sub>O<sub>5</sub> content (> 0.6-1.3%) is found in the glass of the trachybasalts (NAN DR1-2, NAN DR1-3 and NAN DR1-4). This is consistent with the behaviour of P<sub>2</sub>O<sub>5</sub> which decreases in the melt during the crystallization of apatite and K-feldspar. Apparently the plagioclase content of the rocks is depleted with respect to the P<sub>2</sub>O<sub>5</sub> content. The P<sub>2</sub>O<sub>5</sub> readily enters into the lattice of more potassic feldspar as observed in the Na-K feldspar of the trachyte

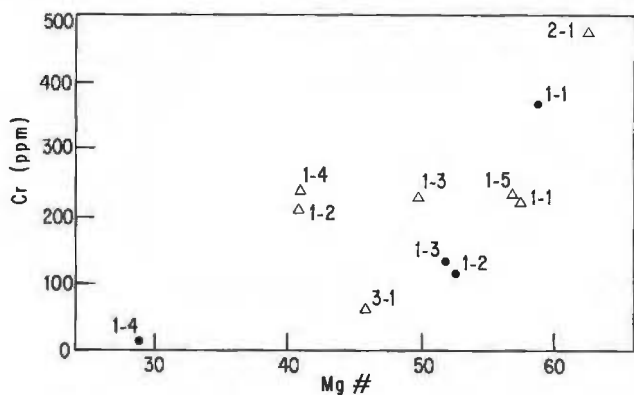


Figure 8  
Mg#-Cr variation diagram of dredged samples from the China Sea seamounts (empty triangles) and from the Manila trench (blacked circles). Samples NAN DR1-4 and NAN DR1-2 ( $\Delta$ ) contain xenoliths.

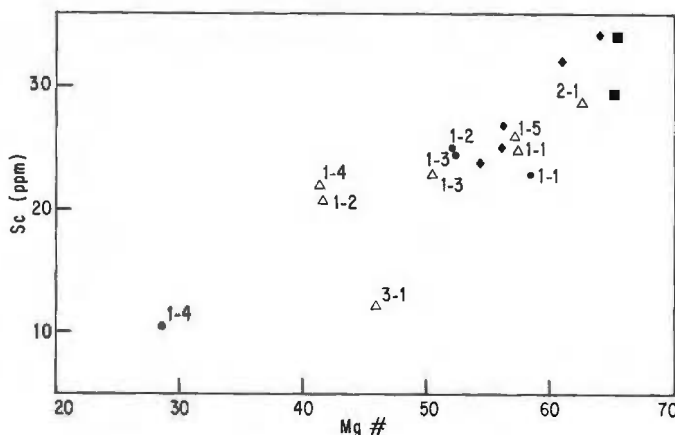


Figure 9  
Mg#-Sc variation diagram of samples from the China Sea seamounts (empty triangles) and from the Manila trench (blacked circles). The black diamonds represent intraplate seamounts from the Eastern Pacific basin (Batiza, Vanko, 1984). The blacked squares are enriched (in incompatible elements) basalts from the East Pacific Rise near 12°50'N.

(EST DR1-4; Tab. 4). Titanomagnetite is prominent as an early-formed phase in the glassy margins of most alkali basalt samples (NAN DR2-1, NAN DR1-2, NAN DR1-4, NAN DR3-1, EST DR1-1 and EST DR1-4).

Compatible elements such as Ni and Cr are strongly partitioned between the least-fractionated melts represented by samples NAN DR2-1, EST DR1-1 and the most evolved rock types such as the trachybasalts NAN DR1-2, NAN DR1-3, NAN DR1-4 and the trachyte (EST DR1-4, Tab. 2). This is also shown by relatively good correlation between the Cr variation and the Mg# of the various rock types (Fig. 8). The Cr content reaches up to 300-500 ppm for the least evolved samples (NAN DR2-1, EST DR1-1), while the trachyte (EST DR1-4) has a Cr content of less than 40 ppm (Tab. 1; Fig. 8). The relatively high values of the Cr (> 200 ppm) for a corresponding low Mg# (40) for the trachybasalts (NAN DR1-4 and NAN DR1-2) is due to the presence of xenolith-xenocryst inclusions (Fig. 8). Sc increases with the Mg# in the melt (Fig. 9). The lowest values (10-22 ppm) are found in the trachyte and trachybasalts, while the least evolved alkali basalts have a Sc content of 22-30 ppm, comparable to that of some EPR axially erupted tholeiitic basalts (Fig. 9).

These latter correspond to relatively high normative clinopyroxene content (Tab. 2).

There is a very small variation in Hf content (3-6 ppm) among the trachybasalts, the alkali olivine basalts, and the plagioclase rich basalts (HPPB; Tab. 2). The trachyte (EST DR1-4) analysed has an Hf content about twice as high as the other types of rocks (Tab. 2). Hf/Yb ratio shows an inverse correlation with the Mg#, and Yb has an affinity for clinopyroxene (Fig. 10). The decrease in Hf/Yb ratios with the increase in Mg# of the liquids (glass) indicates that crystal fractionation resulted in leaving a residue enriched in pyroxene and Fe-enriched mineral phases (Fig. 10).

The rocks analysed from the four dredge hauls have a similar enrichment of the light REE (Tab. 8; Fig. 11). The least evolved olivine alkali basalt (NAN DR2-1, DR1-2, DR1-3) shows a relative depletion in La (< 40 ppm) with respect to the other more evolved alkali basalt. This La depletion reflects the scarcity in pyroxene and plagioclase of the melt. The most fractionated specimens represented by trachyte (EST DR1-4) have the highest values of light REE contents (Tab. 8). Other alkali basalts collected in a similar context to those from the vicinity of the Mariana trench (*i.e.* from the ocean side slope of the Mariana trench (Dietrich *et al.*, 1978), show a comparable  $(La/Sm)_N$  ratio (2-6) to those from the Manila trench (Fig. 10). Intraplate volcanic activity has given rise to these rock types prior to their being subducted into the trench. There is a similarity of the REE distribution pattern for the samples studied here with that of the alkali basalt provinces from intraplate regions of the

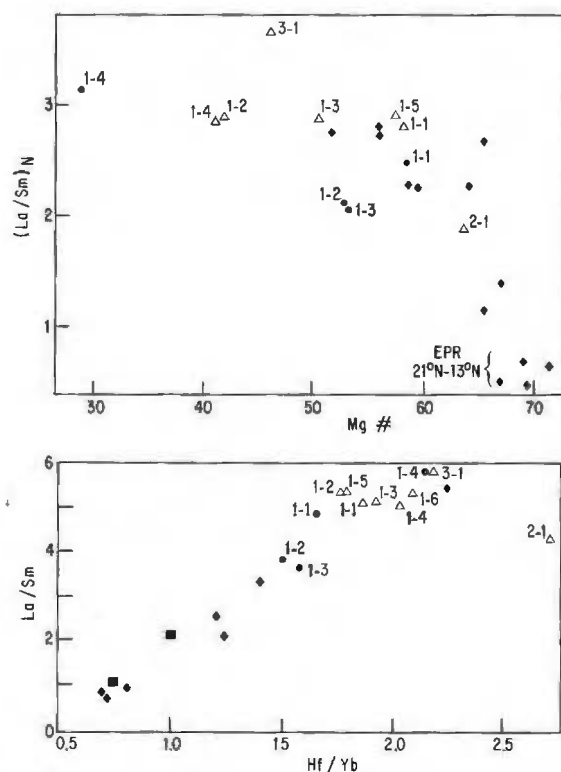


Figure 10  
 $La/Sm$ - $Hf/Yb$  and  $Mg\#(La/Sm)_N$  variation diagram of samples from the China Sea seamounts and the Manila trench compared with other volcanics from Eastern Pacific intraplate seamount and from the accreting plate boundary region of the EPR near 12°50'N. The symbols are the same as in Figure 9.

Table 8

Bulk rare earth analyses of samples from the China Sea (NANHAI) and the Manila trench (ESTASE). The analyses were done by instrumental neutron activation using as reference standards BEN, BCRI and MAGI.

	Estase cruise				Nanhai cruise						
	DR1-1	DR1-2	DR1-3	DR1-4	DR1-6	DR2-1	DR1-3	DR1-1	DR1-2	DR3-1	DR1-4
La	32.55	30.00	23.00	80.00	44.00	23.00	47.00	39.70	36.90	66.00	38.00
Ce	59.26	47.00	49.00	120.00	74.00	67.00	93.00	68.00	54.00	118.00	70.00
Nd	37.00	41.00	30.00	50.00	46.00	30.00	49.00	36.00	36.00	68.00	43.00
Sm	7.40	7.80	6.50	12.70	8.40	5.40	9.30	7.40	7.00	10.30	7.50
Eu	2.30	2.50	2.10	4.80	2.50	1.70	2.60	2.40	2.20	3.10	2.30
Tb	1.10	1.10	1.00	1.70	1.10	0.80	1.30	1.10	1.10	1.10	1.10
Yb	2.70	2.40	2.40	4.50	2.60	2.00	3.00	2.70	2.30	2.90	2.50
Lu	0.50	0.40	0.40	0.40	0.40	0.20	0.50	0.50	0.40	0.50	0.40
	Alk. ol.B.	Alk.	HPPB	Trachyte	Alk.	ol.	Basalt	Trachybasalt			

north-eastern Pacific (Fig. 11). The alkali basalts reported from Batiza and Vanko (1984) from off-axis and intraplate volcanoes near 21°N and 13°N in the eastern Pacific plot are in the same  $(La/Sm)_N$  field as the alkali olivine basalts reported here (Fig. 10).

The alkali basalt suites observed in our study do not fit into the classification of typical calc-alkaline and island arc tholeiitic series as reported in the literature (Jakes, Gill, 1970; Miyashiro, 1974 and others). They do not contain orthopyroxene in equilibrium with the host rock. Instead, they are characterized by high  $K_2O$  (> 2%), high  $TiO_2$  (> 2%) and relatively low  $SiO_2$  (48-50%), except for the trachyte when compared to other calc-alkaline rock series. In addition, their  $P_2O_5$  content (< 1.3%),  $(La/Sm)_N$  ratio (> 2) and  $La/Yb$  ratio (> 10) make them comparable to intraplate and off-axis volcanics encountered in the eastern Pacific Ocean. Both chemical and mineralogical variations observed among the various rock types encountered in the Manila trench and on the China Sea seamounts are interrelated through the partial melting process of comparable upper mantle sources.

#### PETROGENETIC RELATIONSHIP BETWEEN THE VOLCANICS FROM DIFFERENT GEOLOGICAL SETTINGS

As mentioned earlier, previous data from the China Sea seamounts reported by Taylor and Hayes (1983) have indicated the existence of alkali basalts and also intermediate types of basalt with low  $K_2O$  (0.51%). From their available data we interpret these samples as being comparable to our rocks and hence similar to other intraplate volcanics. Their  $Mg\#$  (30-55) is within the same range as the samples reported here (Fig. 4, Tab. 1). Both the alkali basalt suites from the Scarborough seamount chain and those from the wall of the Manila trench are comparable. They differ only in the abundance of foreign inclusions in the alkali basalt suite from the Scarborough seamount chain.

The test for fractional crystallization using the Wright and Doherty (1970) method made between the least evolved sample (NAN DR1-3) and the most evolved specimen (NAN DR1-4) found in the same dredge showed that about 1.3% of olivine ( $Fo_{80}$ ), 6.1% of plagioclase ( $an_{69}$ ), 9.6% ilmenite and trace amounts

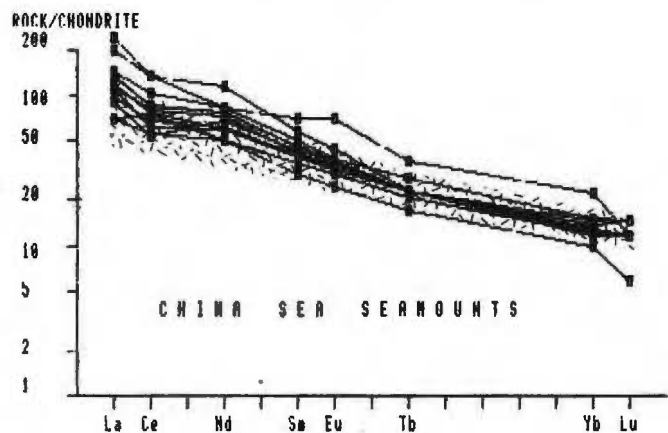


Figure 11

REE normalized to chondrite distribution pattern of the samples from the Manila trench (EST DR1) and from the China Sea seamounts (NAN DR1, DR2, DR3). The shaded area indicates a trend for the North Eastern Pacific intraplate volcanoes (Batiza, Vanko, 1984). (D) Mixing calculation between the least evolved alkali basalt from the China Sea seamount (NAN DR2-1) and the most fractionated trachybasalt (EST DR1-4) from the Manila trench.

(0.03%) of magnetite were necessary for the mass balance calculation. The amount of solid which needs to be crystallized during the fractional crystallization of the alkali basalt suites involving the olivine basalts, the plagioclase rich basalts and the trachybasalts is between 18% and 35%. By the removal of about 5% olivine, 9% clinopyroxene, 25% plagioclase and 8% opaques from an intermediate melt (trachybasalt NAN DR3-1) from the China Sea area, trachytic liquid comparable to that found in the Manila trench (*i.e.* EST DR1-4) could be obtained. The trace element chemical balance calculation used for testing the variability of the crystal fractionation model shows a generally good fit for the large-ion lithophile elements (LIL) such as Ba, Rb and Sr and to some extent for the lanthanides (La, Sm, Yb; Tab. 8, 9). However a major discrepancy (about two-fold) between the observed and calculated values, when the Raleigh fractionation model is applied, exists for the compatible elements such Cr and Ni (Tab. 9). This could be explained by the influence of xenoliths on the bulk rock analyses.

It is likely that the various types of rocks belonging to the alkali basalt suites from the China Sea seamounts and those from the wall (China Sea side) of the Manila trench are cogenetically interrelated and probably were derived from comparable mantle source material. Tra-

Table 9

Trace element chemical balance of evolved alkali-basaltic rocks (NAN DR1-4, EST DR1-3) and trachytes (EST DR1-4) obtained during crystal fractionation of a parental melt similar to NAN DR2-1 and EST DR1-1 respectively (Tab. 2).

	NAN DR1-4 Observed daughter	DR1-4 Calculated daughter	EST DR1-3 Observed	DR1-3 Calculated	EST DR1-4 Observed	DR1-4 Calculated
Ba	407	481	272	251-221	1312	1501-2086
Rb	46	39.7	27	50	100	148-210
Sr	618	668	400	328-288	325	300-120
Ni	—	—	54	121-99	4	60-2
Cr	240	111-78	117	286-258	<10	30-.4
Sc	21.9	21.3	24.3	32	12	30
Hf	5.1	6.5	3.8	6	11	8
La	38	56.3	23	46	80	114-200
Sm	7.5	11	65	11	12.7	20-32
Yb	2.5	3.4	2.4	3.9	4.5	9-14

The partition coefficients used are from Bryan *et al.* (1979); Bryan (1976), Ludden *et al.* (1980), Frey *et al.* (1978), Blanchard *et al.* (1976), Art and Barker (1976). The second set of data was obtained from the Raleigh fractionation law. Single set of data indicates that equilibrium and Raleigh crystallization values are very close.

chYTE was the last phase of the alkali basalt suites to erupt on the sea floor, representing about 12-13% of the fractionated magmatic residue after an important crystallization had taken place beneath each individual volcanic edifice.

## CONCLUSION

The volcanics studied here were collected from two different settings of the China Sea ridge system. One site is located on seamounts formed in the Central China basin area, and the other is located on a subducting crust forming the wall of the Manila trench. All the samples collected consist of rocks belonging to alkali suites. The dredge haul from the Nanhai area with the most recovered samples (NAN DR1) contain rocks with considerable compositional variability, ranging from alkali olivine basalts to more fractionated trachybasalts. The least evolved alkali olivine basalt among all the samples from our collection (NAN DR2-1) was found on a NW-SE elongated seamount (Fig. 2). The rocks collected on an elevated structure located on the top of the Scarborough Seamount chain consist of an evolved trachybasalt (NAN DR3-1).

In the region where the ridge is being subducted into the Manila trench, the dredge haul (EST DR1) consists of the most complete alkali basalt suites showing several stages of magmatic evolution. Alkali basalts, trachybasalts and trachytes were recovered, together with hyaloclastites. At least four types of foreign inclusions (xenoliths and xenocrysts) were found in the alkali basalt suites: 1) a plagioclase-olivine websterite and olivine werlites; 2) sodic (andesine) plagioclase xenocrysts; 3) Mg-rich ( $Fe_{85-88}$ ) olivine xenocrysts; and 4) a gabbroic rock. Some of the most evolved websterites (with a low  $Fe_{78}$  content of its olivine) represent fractionated melts formed in the lower crust during previous magmatic upwelling which gave rise to the

alkali-basalts. Even if tholeiitic basalts were not recovered it is not possible that some Ti-poor pyroxene xenoliths found in alkali basalt could represent cumulates from tholeiitic magmas.

A cogenetic relationship seems to prevail among the samples collected from the same site and also between those from different sites. The samples from different localities of the China Sea ridge could have been derived from the partial melting of similar mantle source material (probably garnet lherzolite). Fractional crystallization during upwelling was the main process involved in differentiating the various rock types encountered. The trachytic flow, also the freshest found on the wall (China Sea side) of the Manila trench was petrologically the last eruptive phase observed among the various volcanic edifices samples. Age-dating based on coccoliths found in the indurated sediment and in the hyaloclastite sampled from the wall of the Manila trench indicates that the subducted crust in the area of sampling is about 11 m.y. old. A comparable age (late Miocene) was obtained for a seamount (NAN DR3, KSO2) located in the central China Sea basin (western part of the Scarborough ridge system).

## Acknowledgements

We are thankful to the captains and the officers and the crew of RV Jean Charcot during the 1984-1985 Nanhai and Estase cruises. The microprobe analyses were carried out by M. Bohn and the thin sections were prepared by G. Floch. Trace and bulk rock analyses were performed by J. Cotten from the Geology Department, Université de Bretagne Occidentale. Drafting and typing of the manuscript were done by J.-P. Mazé and M. Morvan. Dr. R. Maury read the first draft and contributed to its improvement. We are also indebted to J. Boutler and to two anonymous reviewers for their constructive criticism.

## REFERENCES

- Art J. G. and F. Barker (1976). Rare-earth partitioning between hornblende and dacitic liquid and implications for the genesis of trondhjemitic-tonalitic magmas. *Geology*, **4**, 534-536.
- Batiza R. and R. Vanko (1984). Petrology of young Pacific Seamounts. *J. geophys. Res.*, **89**, B13, 11235-11260.
- Blanchard D. P., J. M. Rhodes, M. A. Dungan, K. V. Rodgers, C. H. Donaldson, J. C. Brannon, J. W. Jacobs and E. K. Gibson (1976). The chemistry and petrology of basalts from Leg 37 of the Deep-Sea Drilling Project. *J. geophys. Res.*, **81**, 23, 4231-4246.
- Brooks C. K. (1976). The  $Fe_2O_3/FeO$  ratio of basalt analyses: an appeal for standardized procedure. *Bull. geol. soc. Denmark*, **25**, 117-120.
- Bryan W. B. (1976). A basalt pantellerite association from Isla Socorro Islas Revilla Gigedo. Mexico, In: *Volcanoes and Tectonophase*, H. Aoki and S. Tokai, editors, Univ. Press, 75-91.
- Bryan W. B., G. Thompson and P. J. Michael (1979). Compositional variation in a steady-state zoned magma chamber: Mid-Atlantic Ridge at 36°50' N. *Tectonophysics*, **55**, 63-85.
- Dietrich V., R. Emmermann, R. Oberhansli and H. Puchelt (1978). Geochemistry of basaltic and gabbroic rocks from the west Mariana basin and the Mariana trench. *Earth planet. Sci. Letts*, **39**, 127-144.
- Frey F. A., D. N. Green and S. D. Roy (1978). Integrated models of basalt petrogenesis: a study of quartz tholeiites to olivine melilitites from South Eastern Australia utilizing geochemical and experimental petrological data. *J. Petrology*, **19**, 3, 463-513.
- Hayes D. E. and S. D. Lewis (1985). Structure and tectonics of the Manila Trench system, Western Luzon, Philippines. *Energy*, **10**, 3-4.
- Jakes P. and J. Gill (1970). Rare earth elements and the island arc tholeiitic series. *Earth planet. Sci. Letts*, **9**, 17-28.
- Lewis S. D. and D. E. Hayes (1985). Forearc basin development along western Luzon, Philippines. *Energy*, **10**, 3-4, 281-296.
- Ludden J. N., G. Thompson, W. B. Bryan and F. A. Frey (1980). The origin of lavas from the ninetieth Ridge, eastern Indian ocean: an evaluation of fractional crystallization models. *J. geophys. Res.*, **85**, B8, 4405-4420.
- Martini E. (1971). Standard Tertiary and Quaternary calcareous nannoplankton zonation. *2nd Plankt. Conf. Pro. Rome*, 1970, **2**, 739-785.
- Miyashiro A. (1974). Volcanic rock series in island arcs and active continental margins. *Am. J. Sci.*, **274**, 321-355.
- Okada H. and D. Bukry (1980). Supplementary modifications and introduction of code numbers to the low-latitude coccolith biostratigraphic zonation (Bukry, 1973; 1975). *Mar. Micropaleont.*, **5**, 321-325.
- Pautot G., C. Rangin, A. Briaies, P. Tapponnier, P. Beuzart, G. Lericolais, X. Mathieu, J. Wu, S. Han, H. Li, Y. Lu and J. Zhao (1986). Spreading direction in the central South China Sea. *Nature*, **321**, 150-154.
- Wright T. L. and P. C. Doherty (1970). A linear programming and least squares computer method for solving petrologic mixing problems. *Geol. Soc. Am. Bull.*, **81**, 199-208.

